frontiers in Electronics

ORIGINAL RESEARCH
published: 21 June 2021
doi: 10.3389/felec.2021.703182

Morphological and Optical Tuning of Lead-Free Cs_2SnX_6 (X = I, Br) Perovskite Nanocrystals by Ligand Engineering

Alessandro Veronese[1]*, *Carlo Ciarrocchi*[2], *Marcello Marelli*[3], *Paolo Quadrelli*[2], *Maddalena Patrini*[1] *and Lorenzo Malavasi*[2]*

[1]Department of Physics, University of Pavia, Pavia, Italy, [2]Department of Chemistry and INSTM, University of Pavia, Pavia, Italy, [3]National Research Council, CNR-SCITEC, Milano, Italy

In order to overcome the toxicity of lead halide perovskites, in recent years the research has focused on replacing lead with more environmentally friendly metals like tin, germanium, bismuth or antimony. However, lead-free perovskites still present instability issues and low performances that do not make them competitive when compared to their lead-based counterparts. Here we report the synthesis of lead-free Cs_2SnX_6 (X = Br, I) nanostructures of different shapes by using various surface ligands. These compounds are a promising alternative to lead halide perovskites in which the replacement of divalent lead (Pb(II)) with tetravalent tin (Sn(IV)) causes a modification of the standard perovskite structure. We investigate the effects of different amines on the morphology and size of Cs_2SnX_6 (X = Br, I) nanocrystals, presenting a facile hot-infection method to directly synthesize three-dimensional (3D) nanoparticles as well as two-dimensional (2D) nanoplatelets. The amines not only modify the shape of the crystals, but also affect their optical properties: increasing the length of the amine carbon chain we observe a widening in the bandgap of the compounds and a blue-shift of their emission peak. Alongside the tuning of the chemical composition and the reduction of the crystal size, our study offers a new insight in controlling the physical properties of perovskite nanocrystals by means of the capping ligands, paving the way for future research on lead-free materials.

Keywords: metal halide perovskite, nanocryslalline, ligand engineering, halide alloying, nanostructure

OPEN ACCESS

Edited by:
Aurora Rizzo,
Italian National Research Council, Italy

Reviewed by:
Luisa De Marco,
Italian National Research Council, Italy
Yanqin Li,
Dalian University of Technology, China

***Correspondence:**
Alessandro Veronese
alessandro.veronese02@ateneopv.it
Lorenzo Malavasi
lorenzo.malavasi@unipv.it

Specialty section:
This article was submitted to Optoelectronics, a section of the journal Frontiers in Electronics

Received: *30 April 2021*
Accepted: *03 June 2021*
Published: *21 June 2021*

Citation:
Veronese A, Ciarrocchi C, Marelli M, Quadrelli P, Patrini M and Malavasi L (2021) Morphological and Optical Tuning of Lead-Free Cs_2SnX_6 (X = I, Br) Perovskite Nanocrystals by Ligand Engineering. Front. Electron. 2:703182. doi: 10.3389/felec.2021.703182

INTRODUCTION

In the last decade metal halide perovskites (MHPs) have emerged as a new class of promising semiconductors owing to their peculiar physical properties that make them suitable for different optoelectronic applications. (Fu et al., 2019; Shamsi et al., 2019; Arya et al., 2020; Chouhan et al., 2020; Roy et al., 2020). In particular, the major results of these materials were attained in the photovoltaic field: after just 5 years of research, the efficiency of perovskite solar cells increased from 4 to 20% and they can currently achieve certified values of more than 25%. (Kojima et al., 2009; Stranks and Snaith, 2015; Ono and Qi, 2018; Grancini and Nazeeruddin, 2019; Roy et al., 2020; Best Research-Cell Efficiency Chart | Photovoltaic Research | NREL, 2021).

One of the most remarkable features of MHPs is the possibility to tune their fundamental bandgap by varying their chemical composition over a broad range of energies, from blue to near infrared,

thus producing a wide gamut of emitted colors. (Mittal et al., 2016; Huang et al., 2017a; Chouhan et al., 2020). The tunability of the emission wavelength is also accompanied by low non-radiative recombination rates, as well as high optical absorption coefficients. (De Wolf et al., 2014; Brenner et al., 2016; Ambrosio et al., 2018; Zhang et al., 2018). From the electrical viewpoint, instead, MHPs have demonstrated unusually long carrier lifetimes, resulting in long diffusion lengths and therefore in good charge-transport properties. (Chen et al., 2015; Brenner et al., 2016; Roy et al., 2020). All these features, along with the ease and low cost of processability, contribute to make perovskites a class of very promising and versatile materials, suitable for both light-harvesting and light-emitting applications, and explain the great research interest about them.

In recent years, experimental studies have also focused on nanostructured MHPs, producing a variety of nanocrystals (NCs) in the form of colloidal suspensions. When the size of a crystalline solid is reduced to the nanoscale it starts displaying new properties due to quantum confinement effects, which are not present at macroscopic level. To this regard, MHP NCs offer new appealing features in comparison to their bulk form: they present indeed an extremely high photoluminescence quantum yield, reaching peak values of almost 100%, and very narrow emission linewidths. (Swarnkar et al., 2015; Zhang et al., 2015; Gonzalez-Carrero et al., 2016; Shamsi et al., 2019). Another important advantage of perovskite NCs is their easy compositional tunability: being colloidally dispersed, their chemical composition can be easily modified through facile post-synthetic anion and cation exchange processes. (Akkerman et al., 2015; Nedelcu et al., 2015; Shamsi et al., 2019). Besides, control over size and dimensionality offers a further degree of tunability of the NC optical properties.

The major issue of MHPs is the presence of lead. As a matter of fact, lead-based perovskites are currently the best performing ones, but hazardous lead poses an obstacle to their commercialization in real-life applications. For this reason, more environmentally friendly compounds containing different metals (e.g., Sn, Ge, In, Bi, Sb) are of crucial importance for the future development of perovskite-based technology. (Swarnkar et al., 2017; Creutz et al., 2018; Ju et al., 2018; Sun et al., 2018; Wu et al., 2018; Zhou et al., 2018; Fan et al., 2020; Li et al., 2021). Tin-halide perovskites seem to be a promising alternative to their lead-based counterparts, however they suffer from a severe chemical instability that heavily affects their physical properties. Under ambient conditions Sn(II) tends to easily oxidize into Sn(IV). This undesired process creates trap states that deteriorate the emission properties of the samples. In a recent work by Jellicoe et al., colloidal NCs of $CsSnX_3$ (X = Cl, $Cl_{0.5}Br_{0.5}$, Br, $Br_{0.5}I_{0.5}$, I) were shown to have a very poor quantum yield (less than 0.5%) and a chemical stability of less than 1 h, thus excluding any chance for optoelectronic applications. (Jellicoe et al., 2016).

To overcome the oxidation issue of tin, Sn(II) can be replaced with Sn(IV) and this change in the metal oxidation number leads to the formation of a new crystal structure called vacancy-ordered double perovskite. At present, there are very few reports on Cs_2SnX_6 (X = Cl, Br, I) perovskites in the form of colloidal NCs and even less studies focused on the control over the size and shape of these compounds. To the best of our knowledge, Cs_2SnBr_6 has never been synthesized in the form of colloidal NCs while only a few groups have reported on the synthesis of nanocrystalline Cs_2SnI_6 with results very different from each other. (Wang et al., 2016; Dolzhnikov et al., 2017; Ghosh et al., 2018a; Xu et al., 2019). As a common outcome, however, all groups claimed that the samples were more stable under ambient conditions when compared to the Sn(II)-based compounds, but still with very low quantum yield (less than 1%), thus showing that crystal defects play a crucial role in the emissive processes of these materials.

In this paper, we investigate how the properties of Cs_2SnX_6 (X = Br, I) NCs are affected by different capping agents. The samples are prepared adapting a hot-injection procedure we optimized in a previous study on Sn(IV)-based perovskites. (Veronese et al., 2020). In a typical hot-injection synthesis a mixture of organic acids and amines is employed to passivate the surface of the crystals. Herein, besides the commonly used oleylamine (OLA), we test also hexylamine (C6A), octylamine (C8A), decylamine (C10A) and dodecylamine (C12A) in combination with oleic acid (OA). While OLA leads to the formation of 3D NCs as expected, we observe that shorter chain amines cause a modification of the NC morphology leading to the growth of 2D nanoplatelets (NPs) and we investigated the correlation between the ligand molecule length and the changes in the shape, crystal structure and optical properties of the samples.

RESULTS AND DISCUSSION

NCs of Cs_2SnX_6 (X = Br, I) were synthesized according to the methodology reported in the Experimental Section, which is adapted from a hot injection procedure we developed in a previous study for Cs_2SnX_6 (X = Cl, Br, I) 3D NCs. (Veronese et al., 2020).

X-Ray Diffraction

The crystal structure of the two halide series of NCs is investigated by mean of X-ray diffraction (XRD) and the relative diffraction patterns are reported in **Figure 1**. When OLA is used as capping agent, each sample shows well distinct peaks between 12 and 33° that correspond to the reflections of (111), (220), (222) and (400) planes. Moreover, the peaks of Cs_2SnBr_6 are qualitatively equal to those of Cs_2SnI_6 but shifted to higher angles thus suggesting a reduction of the crystal cell volume as expected since Br^- ions are smaller. This proves that both compounds present one and the same crystal phase that corresponds to the cubic Fm-3m space group (225), as previously reported by our and other groups. (Wang et al., 2016; Jing et al., 2019; Lin et al., 2019; Xu et al., 2019; Veronese et al., 2020). We also evaluated the lattice constants of the two samples being 11.6505 Å and 10.8138 Å for Cs_2SnBr_6 and Cs_2SnI_6, respectively. These results are in line with the data reported in literature and coherent with a decrease of the ionic

radius moving from iodine to bromine. (Kaltzoglou et al., 2016; Saparov et al., 2016; Yuan et al., 2019).

Replacing OLA with shorter amines, instead, leads to dramatic changes in the XRD patterns: the appearance of intense periodic peaks at low angles is the essential evidence of the formation of 2D nanoplatelets. These peaks, which correspond to the (002l) family of crystallographic planes, are indeed the fingerprint of layered structures, indicating a high degree of preferred orientation. In a conventional perovskite, with general formula ABX_3, the metal ion B and the halide X form a cubic array of $[BX_6]^{4-}$ octahedra sharing one corner in all the three directions, while the A ion is situated in the interstitial spaces of this metal halide framework. Vacancy-ordered double perovskites, characterized by the formula A_2BX_6, are a derivative of the standard perovskite structure in which one octahedron is alternatively removed along each of the three axes of the cubic array. In 2D structures, instead, the $[BX_6]^{4-}$ octahedra are still corner sharing but confined in planes separated by the ligand molecules.

Organic acids and amines revealed to be very effective in passivating the surface of colloidal nanomaterials but only when combined. (Huang et al., 2017a; Luo et al., 2017a; Luo et al., 2017b). This phenomenon can be explained by a protonation reaction that takes place between the two organic molecules during the crystal synthesis: an H^+ ion is transferred from the carboxylic group -COOH to the amino group $-NH_2$ generating charged terminations $-COO^-$ and $-NH_3^+$ in the molecules that can bind to the crystal surface ions. (De Roo et al., 2016; Huang et al., 2017b; Almeida et al., 2018; Yang et al., 2018). In this framework, the protonated amine moiety attaches to the halogen anions through hydrogen bonding and can stick into the crystal lattice between the tin(IV) halide layers thus keeping them separated. (Xu et al., 2003; Xiao et al., 2018).

From the diffractograms we can see that when C6A is used in place of OLA it leads again to the formation of 3D nanocrystals. In the case of Cs_2SnI_6, however, the coexistence of layered structures is also detected as revealed by the peaks at 4.51, 17.89 and 22.41°. Moving from C6A to C8A, the patterns appear very different: 2D phases are now predominant with well distinguishable peaks at low angles while the 3D phase disappears in the I-based samples and just small traces are present in the Br-based ones. Finally, a further increasing of the amine molecule length results in the complete vanishing of the 3D phase and only the NP peaks are now detectable. When only OA is used as ligand, instead, we observed that the synthesis leads to 3D NCs, but they do not present any photoluminescence emission. The formation of different crystal structures is related to a competition between the Cs^+ ions and the alkylammonium ions to bind to the inorganic octahedra during the nanocrystal growth. (Ravi et al., 2017; Almeida et al., 2018). The prevalence of NPs over NCs in a synthesis depends on the ratio between amine and Cs, the amine binding affinity for the tin(IV) halide and the acid-base equilibrium between the ligands. (Fanizza et al., 2019; Xu et al., 2019). When the pH decreases, the amine molecules protonate and the concentration of alkylammonium raises. This unbalances the reaction at the expense of Cs and the growth of 2D structures is promoted. The appearance in our samples of different crystal phases depending on the halogen may be due to the different binding affinity of the amines with the two halides; this aspect requires further investigation to understand the correlation between the amine length and the crystal morphology and its origin.

Interestingly, we notice in almost every sample the presence of cesium halide. This can be due to the excess of tin(IV) halide used during the syntheses. As mentioned above, when the amino group of the capping molecules bonds to the octahedra layers it takes in fact the position of the A cation, so the Cs^+ ions that do not enter into the lattice can react with the excess halogen in the solution producing the halide salts we detect. These results show already a clear evidence of the influence of capping agents on the structure of nanocrystals.

Electron Microscopy

These changes revealed by XRD are confirmed in crystal shape and morphology by high resolution transmission electron microscopy (HRTEM). The images taken for the 3D samples, reported in **Figures 2A,B**, show that the synthesis with OLA leads to spherical nanoparticles with a diameter of about 3 nm and a narrow size distribution, accordingly with previous studies on Cs_2SnI_6 NCs. (Wang et al., 2016; Ghosh et al., 2018b; Veronese et al., 2020). In the case of shorter amines, HRTEM analysis reveals remarkably different properties. The C6A sample of the iodine series, as previously shown by XRD measurements, presents a mixed phase composed of spherical NCs and 2D nanobelts, namely planar structures elongated in one direction with lateral size of hundreds of nanometers (**Figures 2C,D** and **Supplementary Figure S1A**). In particular, the NCs display similar features to those synthesized with OLA but are characterized by a bigger diameter of about 10 nm. The C12A sample, instead, consists only of a 2D phase with NPs of hexagonal or square shape. This planar morphology reflects the layered crystal structure that was detected by XRD measurements. Contrary to 3D crystals, here the platelets appear more varied presenting different shapes and a wide size distribution ranging from 10 to almost 100 nm (**Figures 2E,F** and **Supplementary Figure S1B**). Both samples show a high degree of crystallinity as verified by electron diffraction (**Supplementary Figures S3A,B**). These results are in agreement with the only literature data on Cs_2SnI_6 2D layered structures by Xu et al. where they obtained hexagonal NPs with lateral size of several hundreds of nanometers. (Xu et al., 2019).

The analysis on the Cs_2SnBr_6 series leads to similar results, although with some substantial differences, which are collected in the **Supporting Information** (**SI**) section along with additional TEM images. The C6A sample presents aggregates that appear made of spherical NCs of the order of 50 nm, with no planar structures like the previous nanobelts (**Supplementary Figures S2A,B**). The C12A sample, instead, shows only 2D NPs with lateral size of hundreds of nanometers (**Supplementary Figures S2C–E**). As mentioned, contrary to the I series the Cs_2SnBr_6 crystals exhibit a high tendency to agglomerate forming clusters of great size. However, the electron diffraction reveals that also these samples are highly crystalline (**Supplementary Figures S3C,D**). The cause of this phenomenon is unclear. In general,

the colloidal stability of nanocrystals is a multifactorial issue that depends on the nature of the compound, the ligands and the suspension solvent and it is determined by a balance between attractive and repulsive interparticle forces. (Boles et al., 2016). The aggregation of the Br-based samples could be related to a different interaction between halide and amines that makes the ligand binding to the crystal surface more labile, but its origin and mechanisms are still unknown and thorough investigations are needed to understand them.

The HRTEM instrumentation allowed also to perform energy dispersive X-ray (EDX) analysis to investigate the chemical composition of the samples. Representative X-ray spectra of NPs, along with their EDX elemental maps, are reported in **Supplementary Figures S4, S5, S6** of the **SI** and they show the clear presence of the three constituting elements of each perovskite, thus confirming the formation of the compounds revealed by XRD.

Absorption

The length of the amine carbon chain not only affects the morphology of the crystals but also their optical properties. The absorption spectra of both I and Br series are reported in **Figure 3**. From a qualitative analysis, the NP spectra appear significantly different when compared to those of their 3D counterparts: they present a slow rise across the entire visible range and a rapid increase in the UV region. Moreover, differently from Pb-based NCs, none of the samples have a sharp excitonic absorption peak, but rather they display a long tail toward the low energies. This feature has been previously reported also for Sn(IV)-based perovskite thin films and it was attributed to the presence of crystal defects (most likely halide vacancies since they have a low formation energy) that introduce a sizable density of shallow electronic states below the conduction band (CB) edge. (Xiao et al., 2015; Maughan et al., 2016; Saparov et al., 2016). In the case of Cs_2SnBr_6, we notice also that the C6A and C8A samples show a peak around 360 nm, similarly to their 3D counterparts, which disappears for the longer amines. This difference can be explained by the exclusive presence of the 3D phase in these samples, as we have inferred from XRD measurements.

From the Tauc plots for direct bandgap of the absorption spectra the value of the energy bandgap is derived, as reported in **Supplementary Table S1**. For 3D NCs synthesized with OLA, Cs_2SnI_6 and Cs_2SnBr_6 are found to have gaps of 1.57 and 3.33 eV, that are higher than those of their relative bulk forms (1.3 and 2.7 eV, respectively). (Kaltzoglou et al., 2016; Yuan et al., 2019). Moving to 2D structures, on the other hand, we can observe that the gap energy becomes even higher, increasing linearly with increasing the amine length (**Figure 4**). These results can be ascribed to quantum confinement effects caused by the small size of the crystals consistently with previous studies on Cs_2SnI_6 NCs. (Wang et al., 2016; Dolzhnikov et al., 2017; Xu et al., 2019; Veronese et al., 2020). In particular, being made of a few atomic layers, perovskite NPs are reported to have very strong exciton confinement, thus explaining their larger increment of the bandgap. (Tyagi et al., 2015; Weidman et al., 2017; Wang et al., 2018). Besides the case of NPs, the gap energy of 3D NCs synthesized with short amines is also evaluated from Tauc plot extrapolations. In the case of Cs_2SnI_6 sample with C6A, where mixed phase is present, the gap of 3D phase is estimated at 1.54 eV. The NCs of the C6A and C8A samples with Br, instead, are found to have a gap energy of 3.13 and 3.25 eV, respectively. All these values are reasonably close to those of NCs prepared with OLA: the differences can be ascribed to the larger diameter of the crystals causing a smaller size effect.

Photoluminescence

Light emission is also affected by the change in the nanocrystal dimensionality. As it is evident from the photoluminescence (PL) spectra of **Figure 5**, replacing OLA with shorter amines results in a blue-shift of the emission, which is particularly evident in the case of I compounds where the emission color changes from dark red to orange. The 3D NCs of Cs_2SnI_6 and Cs_2SnBr_6 present PL peak emission at $\lambda = 790$ and 603 nm, respectively. Moving from C8A to C12A, the emission of Cs_2SnBr_6 NPs shifts from 599 to 575 nm following a linear trend. In the case of Cs_2SnI_6, instead, the NP spectra are peaked at 635, 624, and 628 nm. Remarkably, the samples synthesized with C6A of both halide series do not show any emission.

In the synthesis of nanomaterials, ligands play a crucial role in stabilizing the crystals. In fact, they are necessary not only to passivate the surface of the NCs—restoring dangling bonds and so preventing the consequent defect states within the bandgap—but also to create a protective layer that shields them from detrimental external agents. (Heuer-Jungemann et al., 2019). Moreover, the chemical stability of NCs depends on the shape of ligand molecules: long and branched molecules were demonstrated to achieve the best results in stabilizing nanomaterials. (Luo et al., 2017a; Yang et al., 2018; Kumar et al., 2019; Xie et al., 2019). In this regard, the lack of emission from the C6A samples can be attributed to a poor stabilization of the amine resulting in the formation of defect states that quench the PL radiative process. We notice that the emission energy peak of each sample is significantly lower than the value found for its energy gap. Coherently with the wide tail observed in the absorption spectra, this large Stokes shift may be caused by a high density of electronic states, arising from crystal defects, that locate right below the CB minimum: when the electrons are excited into the CB, they thermalize toward the edge, transfer into the defect states, and finally decay in the valence band with radiative emission of light. This phenomenon requires further investigation to be fully understood.

Due to the asymmetry of the curve, the PL spectra were fitted using two Gaussian lineshapes thus revealing a second peak at longer wavelengths, from 729 to 717 nm for the I samples and from 697 to 642 nm for the Br compounds (**Supplementary Figure S8**). The corresponding energy values of the two emission peaks are reported in **Figure 6** and **Supplementary Table S1**. Accordingly with previous study by Xu et al. on Cs_2SnI_6 2D NPs, the peak emerging at lower energy may be ascribed to an emission from defect states. (Xu et al., 2019). In their work, indeed, Xu and coworkers attributed the origin of such defects to a structural distortion caused by a phase transition between two layered structures based on orthorhombic and monoclinic unit cells.

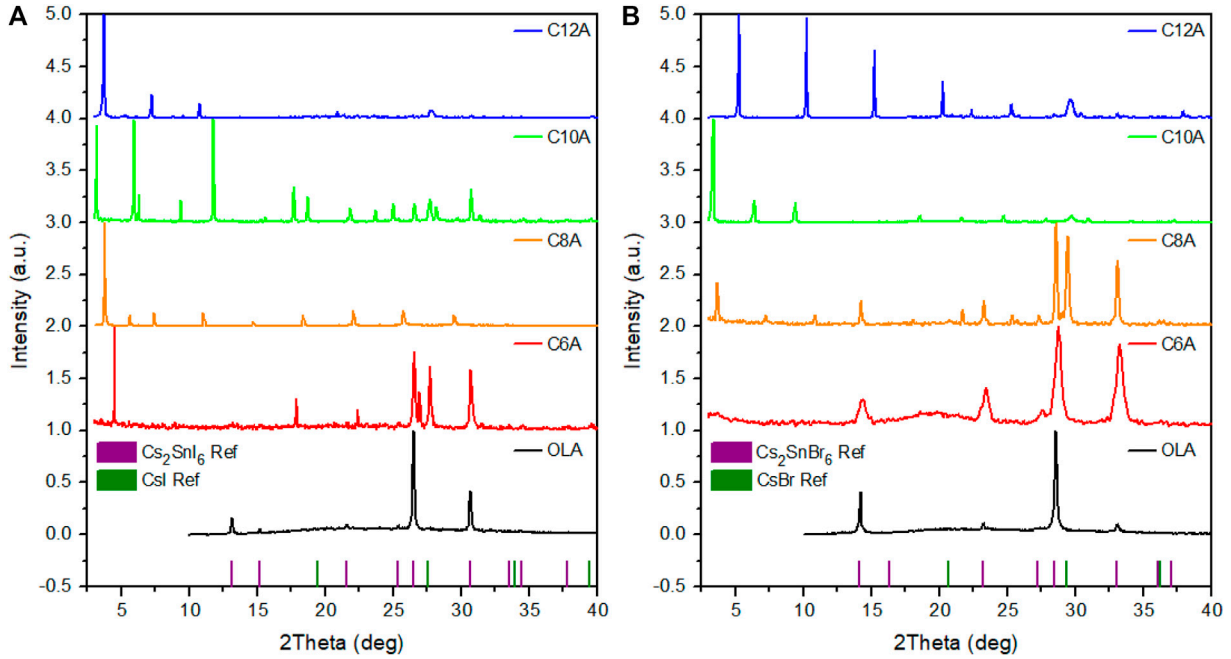

FIGURE 1 | XRD patterns of Cs_2SnI_6 **(A)** and Cs_2SnBr_6 **(B)** samples synthesized with different amines.

This lattice distortion should modulate the formation energies of the defects while the spatial shifts of the ligand molecules, altering the bonding between the amino group and the halide octahedra, can generate more crystal defects. This phenomenon has already been observed in Pb(II)- and Sn(IV)-based 2D layered perovskites (Okuda et al., 1993; Pradeesh et al., 2009; Dohner et al., 2014; Cortecchia et al., 2017) and can be consistent with our previous observations on large Stokes shifts in emission and wide tails in absorption. However, in order to fully reveal the link between these three aspects and their exact origin further studies are needed.

CONCLUSION

In summary, we developed a facile hot-injection method that allows to synthesize simultaneously 3D nanocrystals and 2D nanoplatelets for both Cs_2SnI_6 and Cs_2SnBr_6 perovskites. The crystal morphology is tuned by changing the amine employed as capping agent during the synthetic procedure. When using OLA, the most common amine widely employed in literature, the synthesis leads to spherical NCs with a very small diameter of about 3 nm. When using amines with a shorter carbon chain, instead, the results are very different and the synthesis leads to 2D layered NPs with diverse crystal structures depending on the ligand used, as demonstrated by XRD and TEM analyses. The change in the morphology of the crystals is also followed by a modification of their optical properties. Thanks to the reduced size, all the samples present a much wider bandgap in comparison to their bulk form due to strong quantum confinement effects, so that the NP gap energy linearly shifts from 1.3 to 2.87 eV in the case of Cs_2SnI_6 and from 2.7 to 4.32 eV in the case of Cs_2SnBr_6. Besides, light emission is also affected by the ligand choice and changing the amines allows to tune the emission of Cs_2SnI_6 samples from 1.57 to 1.99 eV moving from 3D NCs to 2D NPs, and analogously from 2.06 to 2.16 eV nm for the Cs_2SnBr_6 samples. These results present an interesting advance in the research on perovskite nanocrystals toward lead-free compounds and offer a further insight in Sn(IV)-based double perovskites for possible future applications in optoelectronic devices.

EXPERIMENTAL SECTION

Chemicals

Cs_2CO_3 (Acros Organics, 99.995%), $SnBr_4$ (Sigma-Aldrich, 99%), SnI_4 (Sigma-Aldrich, 99.999%), 1-octadecene (ODE, Acros Organics, 90%), oleic acid (OA, VWR Chemicals, 81%), oleylamine (OLA, Acros Organics, 80–90%), hexylamine (C6A, Sigma-Aldrich, ≥99%), octylamine (C8A, Sigma-Aldrich, 99%), decylamine (C10A, Sigma-Aldrich, 95%), dodecylamine (C12A, Sigma-Aldrich, 98%), hexane (HEX, Sigma-Aldrich ≥99%). All reagents were used without further purification.

Synthesis

Synthesis of Cs-oleate: 4.5 ml of ODE and 0.5 ml of OA were loaded in a 50 ml three-neck flask and dried under vacuum at 120°C for 1 h. Subsequently, 0.1625 g of Cs_2CO_3 was added to the mixture and the solution was dried again under vacuum at the same temperature for one additional hour. Finally, the flask

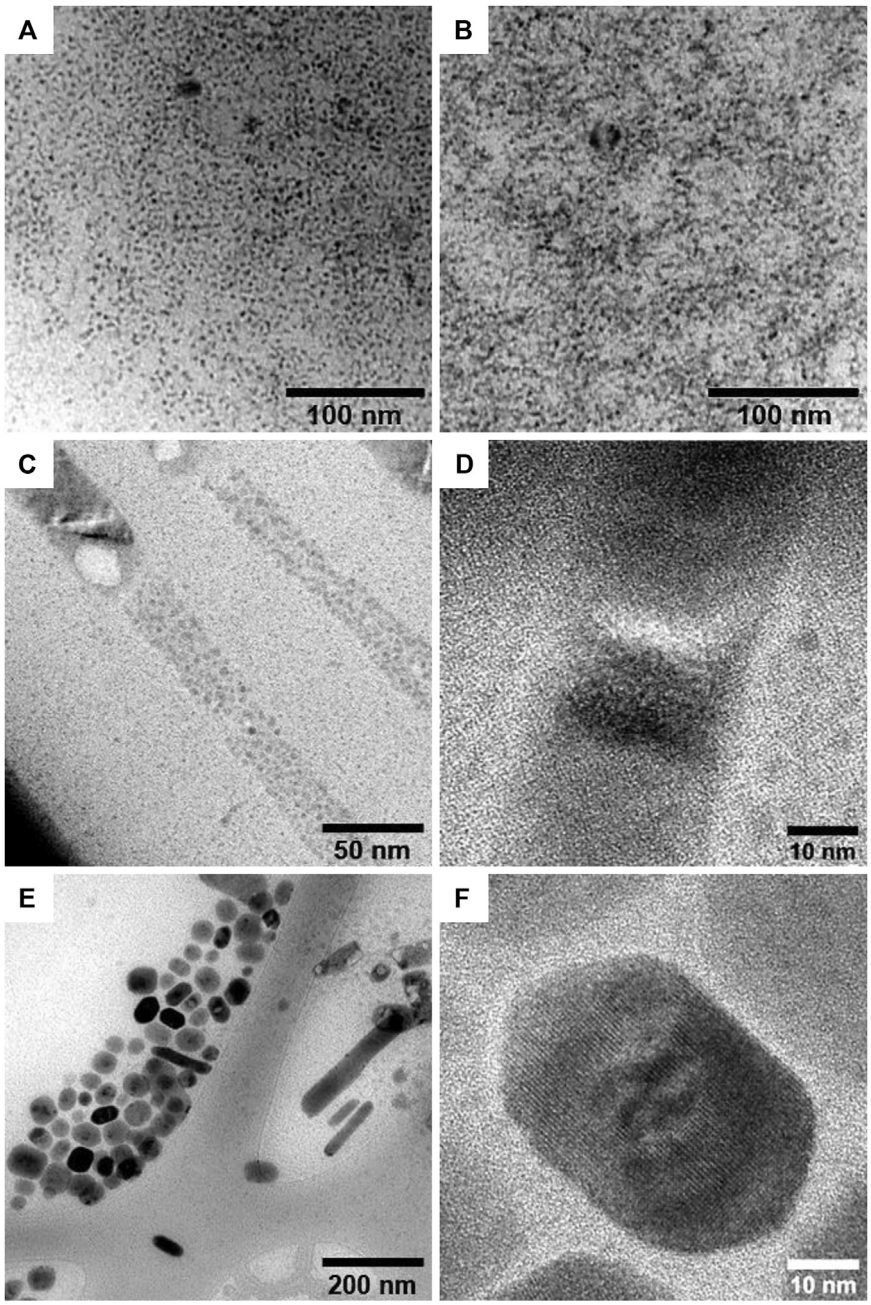

FIGURE 2 | TEM images of OLA synthesized NCs of Cs_2SnI_6 **(A)** and Cs_2SnBr_6 **(B)**, and HRTEM images of Cs_2SnI_6 samples synthesized with C6A **(C, D)** and C12A **(E, F)**.

was heated at 150°C under nitrogen flow until complete dissolution of Cs_2CO_3 (approximately 1 h). Since Cs-oleate is insoluble in ODE at room temperature, the precursor solution was preheated at 100°C before use to completely dissolve the precipitate.

Synthesis of Cs_2SnX_6 (X = Br, I) NCs: 5 ml of ODE were loaded in a 50 ml three-neck flask with 0.2 ml of OA and 0.2 ml of OLA and the mixture was degassed under vacuum at 120°C for 1 h. Subsequently, 0.235 mmol of SnX_4 (0.1027 g of $SnBr_4$ and 0.1468 g of SnI_4, respectively) was added to the flask and the solution was dried under vacuum at 80°C for 15 min. The flask was then moved under nitrogen flow and heated up to 220°C. As soon as it reaches the desired temperature, 0.5 ml of the as-prepared Cs-oleate solution was quickly injected in the reaction vessel and after 1 min it was cooled down in an ice bath. To purify the NCs, 2.5 ml of HEX was added to the mother solution, the mixture was centrifugated at 7000 rpm for 5 min and the surfactant was discarded. Part of the crystals

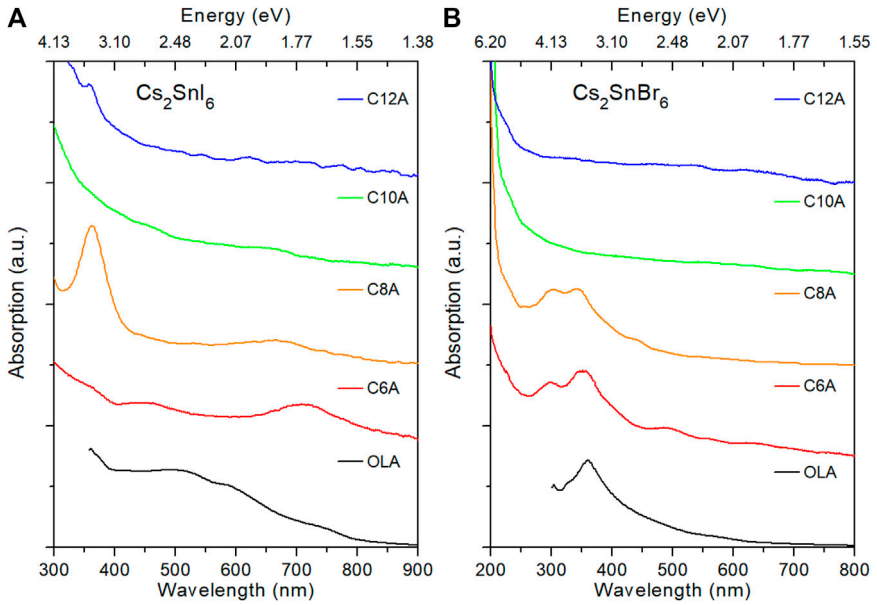

FIGURE 3 | Absorption spectra of Cs_2SnI_6 **(A)** and Cs_2SnBr_6 **(B)** samples synthesized with different amines. (Curves were shifted vertically for clarity).

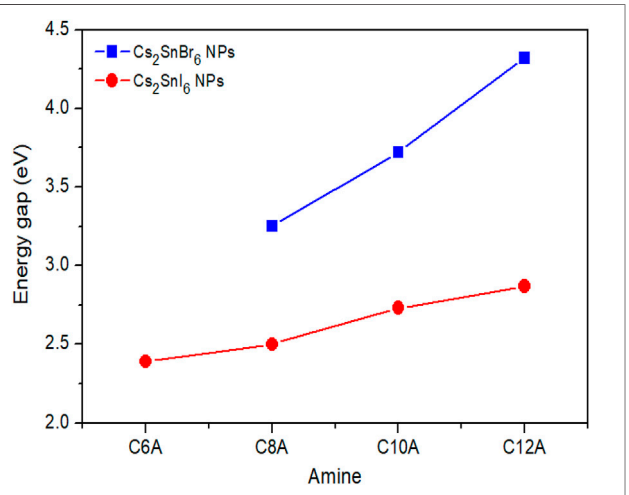

FIGURE 4 | Fundamental energy gap of 2D NPs as a function of the amine length used as capping agent. (Lines are just a guide for the eye).

was then deposited on glass slides for future measures while the rest crystals was dispersed in 5 ml of HEX. All the synthetic and purification processes were conducted under ambient conditions and no argon-filled glovebox was used to store the final samples.

Synthesis of Cs_2SnX_6 (X = Br, I) NPs: the synthesis of nanoplatelets follows the same procedures illustrated for the 3D NCs except that 0.2 ml of the desired amine was used in place of OLA. The mother solution was finally purified by centrifugation at 7000 rpm for 5 min after adding 2.5 ml of HEX and the resulting samples were stored under ambient conditions.

High Resolution Transmission Electron Microscopy

High resolution transmission electron microscopy (HRTEM) was performed on a ZEISS LIBRA200FE equipped with a high-angle annular dark-field (HAADF) detector for STEM (scanning TEM) mode. Energy dispersive X-ray (EDX) analysis was conducted on the same instrument using an Oxford X-stream two probe. The specimens were prepared by depositing 8 µl of the sample dispersed in HEX on a copper grid covered with a double carbon film and letting the solvent evaporate in air. The size of the samples was measured from TEM images using ImageJ 1.52a software.

X-Ray Diffraction

X-ray diffraction (XRD) measurements were performed under ambient condition on a Bruker D8 Advance diffractometer in the Bragg-Brentano configuration using copper Kα radiation (λ = 1.54056 Å) as X-ray source. The diffractograms were recorded from 3 to 40°, with resolution of 0.04° and integration time of 4 s. The specimens were prepared by depositing the sample on a glass slide with a spatula and spreading it thoroughly in order to get a smooth surface. The reference patterns were calculated with PowderCell 2.4 software using the literature data specified in the text as references.

Absorption Spectroscopy

Ultraviolet-Visible (UV-Vis) absorption measurements were performed under ambient conditions using a Varian Cary 50 spectrophotometer equipped with a Xe lamp as light source, a silicon photodiode as detector and a Czerny-Turner monochromator with fixed spectral bandwidth of 1.5 nm. The spectra were recorded from 200 to 1,000 nm, with resolution of 2 nm and integration time of 0.5 s. The specimens were prepared

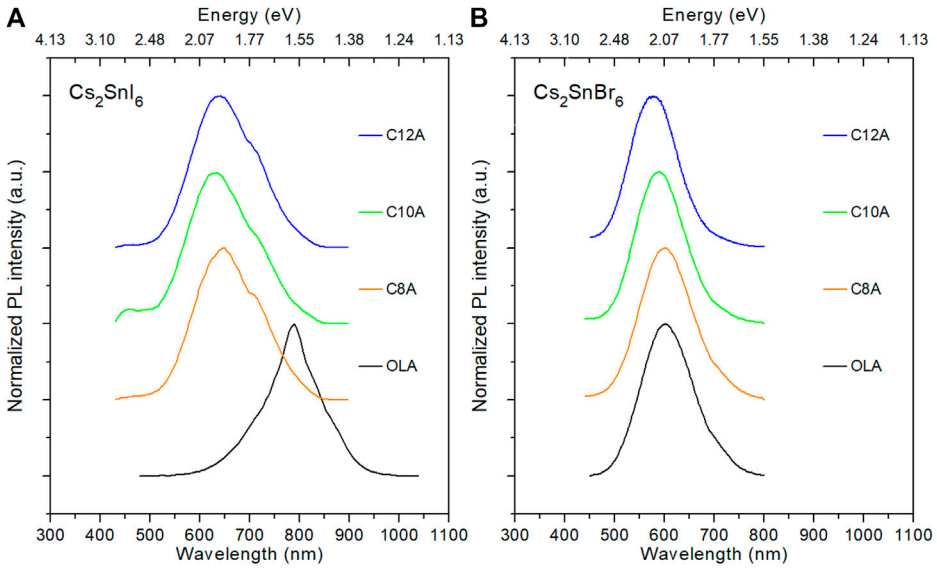

FIGURE 5 | PL spectra of Cs_2SnI_6 **(A)** and Cs_2SnBr_6 **(B)** samples synthesized with different amines. (Curves were shifted vertically for clarity).

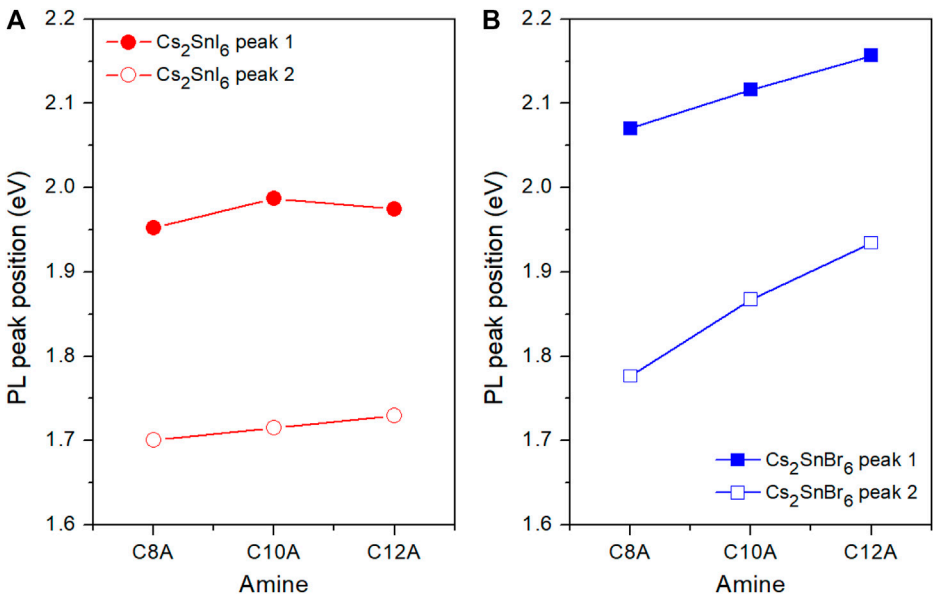

FIGURE 6 | Energy of the PL peaks of Cs_2SnI_6 **(A)** and Cs_2SnBr_6 **(B)** 2D NPs. (Lines are just a guide for the eye).

by loading the samples into quartz cuvettes with 1 cm optical path. The baseline was taken using the cuvettes filled with HEX as reference.

Steady-State Photoluminescence Spectroscopy

PL measurements were performed under ambient conditions using Varian Cary Eclipse fluorescence spectrophotometer equipped with Xe lamp as light source, a photomultiplier as detector and two Czerny-Turner monochromators with limiting resolution of 1.5 nm. The spectra were recorded exciting the samples at 360 nm wavelength. The specimens were prepared by loading the samples into quartz cuvettes with 1 cm optical path. To find the emission peaks, the PL spectra were fitted with two Gaussian lineshapes using OriginLab Origin 8.1 software.

DATA AVAILABILITY STATEMENT

The original contributions presented in the study are included in the article/**Supplementary Material**, further inquiries can be directed to the corresponding authors.

AUTHOR CONTRIBUTIONS

AV prepared the samples and performed XRD and absorbance measurements; PQ assisted the sample preparation and data discussion; MM carried out TEM analysis; CC performed PL measurements; MP and LM devised the research and coordinated the work, AV, LM, and MP wrote the manuscipt.

SUPPLEMENTARY MATERIAL

The Supplementary Material for this article can be found online at: https://www.frontiersin.org/articles/10.3389/felec.2021.703182/full#supplementary-material

REFERENCES

Akkerman, Q. A., D'Innocenzo, V., Accornero, S., Scarpellini, A., Petrozza, A., Prato, M., et al. (2015). Tuning the Optical Properties of Cesium Lead Halide Perovskite Nanocrystals by Anion Exchange Reactions. *J. Am. Chem. Soc.* 137, 10276–10281. doi:10.1021/jacs.5b05602

Almeida, G., Goldoni, L., Akkerman, Q., Dang, Z., Khan, A. H., Marras, S., et al. (2018). Role of Acid-Base Equilibria in the Size, Shape, and Phase Control of Cesium Lead Bromide Nanocrystals. *ACS Nano*. 12, 1704–1711. doi:10.1021/acsnano.7b08357

Ambrosio, F., Wiktor, J., De Angelis, F., and Pasquarello, A. (2018). Origin of Low Electron-Hole Recombination Rate in Metal Halide Perovskites. *Energy Environ. Sci.* 11, 101–105. doi:10.1039/c7ee01981e

Arya, S., Mahajan, P., Gupta, R., Srivastava, R., Tailor, N. k., Satapathi, S., et al. (2020). A Comprehensive Review on Synthesis and Applications of Single crystal Perovskite Halides. *Prog. Solid State. Chem.* 60, 100286. doi:10.1016/j.progsolidstchem.2020.100286

Best Research-Cell Efficiency Chart | Photovoltaic Research | NREL (2021). Available at: https://www.nrel.gov/pv/cell-efficiency.html (accessed 11/01/2021).

Boles, M. A., Ling, D., Hyeon, T., and Talapin, D. V. (2016). The Surface Science of Nanocrystals. *Nat. Mater.* 15, 141–153. doi:10.1038/nmat4526

Brenner, T. M., Egger, D. A., Kronik, L., Hodes, G., and Cahen, D. (2016). Hybrid Organic—Inorganic Perovskites: Low-Cost Semiconductors with Intriguing Charge-Transport Properties. *Nat. Rev. Mater.* 1, 15007. doi:10.1038/natrevmats.2015.7

Chen, Q., De Marco, N., Yang, Y., Song, T.-B., Chen, C.-C., Zhao, H., et al. (2015). Under the Spotlight: The Organic-Inorganic Hybrid Halide Perovskite for Optoelectronic Applications. *Nano Today*. 10, 355–396. doi:10.1016/j.nantod.2015.04.009

Chouhan, L., Ghimire, S., Subrahmanyam, C., Miyasaka, T., and Biju, V. (2020). Synthesis, Optoelectronic Properties and Applications of Halide Perovskites. *Chem. Soc. Rev.* 49, 2869–2885. doi:10.1039/c9cs00848a

Cortecchia, D., Neutzner, S., Srimath Kandada, A. R., Mosconi, E., Meggiolaro, D., De Angelis, F., et al. (2017). Broadband Emission in Two-Dimensional Hybrid Perovskites: The Role of Structural Deformation. *J. Am. Chem. Soc.* 139, 39–42. doi:10.1021/jacs.6b10390

Creutz, S. E., Crites, E. N., De Siena, M. C., and Gamelin, D. R. (2018). Colloidal Nanocrystals of Lead-Free Double-Perovskite (Elpasolite) Semiconductors: Synthesis and Anion Exchange to Access New Materials. *Nano Lett.* 18, 1118–1123. doi:10.1021/acs.nanolett.7b04659

De Roo, J., Ibáñez, M., Geiregat, P., Nedelcu, G., Walravens, W., Maes, J., et al. (2016). Highly Dynamic Ligand Binding and Light Absorption Coefficient of Cesium Lead Bromide Perovskite Nanocrystals. *ACS Nano*. 10, 2071–2081. doi:10.1021/acsnano.5b06295

De Wolf, S., Holovsky, J., Moon, S.-J., Löper, P., Niesen, B., Ledinsky, M., et al. (2014). Organometallic Halide Perovskites: Sharp Optical Absorption Edge and its Relation to Photovoltaic Performance. *J. Phys. Chem. Lett.* 5, 1035–1039. doi:10.1021/jz500279b

Dohner, E. R., Jaffe, A., Bradshaw, L. R., and Karunadasa, H. I. (2014). Intrinsic White-Light Emission from Layered Hybrid Perovskites. *J. Am. Chem. Soc.* 136, 13154–13157. doi:10.1021/ja507086b

Dolzhnikov, D. S., Wang, C., Xu, Y., Kanatzidis, M. G., and Weiss, E. A. (2017). Ligand-Free, Quantum-Confined Cs2SnI6 Perovskite Nanocrystals. *Chem. Mater.* 29, 7901–7907. doi:10.1021/acs.chemmater.7b02803

Fan, Q., Biesold-McGee, G. V., Ma, J., Xu, Q., Pan, S., Peng, J., et al. (2020). Lead-Free Halide Perovskite Nanocrystals: Crystal Structures, Synthesis, Stabilities, and Optical Properties. *Angew. Chem. Int. Ed.* 59, 1030–1046. doi:10.1002/anie.201904862

Fanizza, E., Cascella, F., Altamura, D., Giannini, C., Panniello, A., Triggiani, L., et al. (2019). Post-synthesis Phase and Shape Evolution of CsPbBr3 Colloidal Nanocrystals: The Role of Ligands. *Nano Res.* 12, 1155–1166. doi:10.1007/s12274-019-2371-2

Fu, Y., Zhu, H., Chen, J., Hautzinger, M. P., Zhu, X.-Y., and Jin, S. (2019). Metal Halide Perovskite Nanostructures for Optoelectronic Applications and the Study of Physical Properties. *Nat. Rev. Mater.* 4, 169–188. doi:10.1038/s41578-019-0080-9

Ghosh, S., Paul, S., and De, S. K. (2018a). Control Synthesis of Air-Stable Morphology Tunable Pb-free Cs2 SnI6 Perovskite Nanoparticles and Their Photodetection Properties. *Part. Part. Syst. Charact.* 35, 1800199. doi:10.1002/ppsc.201800199

Ghosh, S., Shi, Q., Pradhan, B., Kumar, P., Wang, Z., Acharya, S., et al. (2018b). Phonon Coupling with Excitons and Free Carriers in Formamidinium Lead Bromide Perovskite Nanocrystals. *J. Phys. Chem. Lett.* 9, 4245–4250. doi:10.1021/acs.jpclett.8b01729

Gonzalez-Carrero, S., Francés-Soriano, L., González-Béjar, M., Agouram, S., Galian, R. E., and Pérez-Prieto, J. (2016). The Luminescence of CH3NH3PbBr3Perovskite Nanoparticles Crests the Summit and Their Photostability under Wet Conditions Is Enhanced. *Small.* 12, 5245–5250. doi:10.1002/smll.201600209

Grancini, G., and Nazeeruddin, M. K. (2019). Dimensional Tailoring of Hybrid Perovskites for Photovoltaics. *Nat. Rev. Mater.* 4, 4–22. doi:10.1038/s41578-018-0065-0

Heuer-Jungemann, A., Feliu, N., Bakaimi, I., Hamaly, M., Alkilany, A., Chakraborty, I., et al. (2019). The Role of Ligands in the Chemical Synthesis and Applications of Inorganic Nanoparticles. *Chem. Rev.* 119, 4819–4880. doi:10.1021/acs.chemrev.8b00733

Huang, H., Bodnarchuk, M. I., Kershaw, S. V., Kovalenko, M. V., and Rogach, A. L. (2017). Lead Halide Perovskite Nanocrystals in the Research Spotlight: Stability and Defect Tolerance. *ACS Energ. Lett.* 2, 2071–2083. doi:10.1021/acsenergylett.7b00547

Huang, H., Raith, J., Kershaw, S. V., Kalytchuk, S., Tomanec, O., Jing, L., et al. (2017). Growth Mechanism of Strongly Emitting CH3NH3PbBr3 Perovskite Nanocrystals with a Tunable Bandgap. *Nat. Commun.* 8, 996. doi:10.1038/s41467-017-00929-2

Jellicoe, T. C., Richter, J. M., Glass, H. F. J., Tabachnyk, M., Brady, R., Dutton, S. E., et al. (2016). Synthesis and Optical Properties of Lead-Free Cesium Tin Halide Perovskite Nanocrystals. *J. Am. Chem. Soc.* 138, 2941–2944. doi:10.1021/jacs.5b13470

Jing, Y., Liu, Y., Zhao, J., and Xia, Z. (2019). Sb3+ Doping-Induced Triplet Self-Trapped Excitons Emission in Lead-Free Cs2SnCl6 Nanocrystals. *J. Phys. Chem. Lett.* 10, 7439–7444. doi:10.1021/acs.jpclett.9b03035

Ju, M.-G., Chen, M., Zhou, Y., Garces, H. F., Dai, J., Ma, L., et al. (2018). Earth-Abundant Nontoxic Titanium(IV)-based Vacancy-Ordered Double Perovskite

Halides with Tunable 1.0 to 1.8 eV Bandgaps for Photovoltaic Applications. *ACS Energ. Lett.* 3, 297–304. doi:10.1021/acsenergylett.7b01167

Kaltzoglou, A., Antoniadou, M., Kontos, A. G., Stoumpos, C. C., Perganti, D., Siranidi, E., et al. (2016). Optical-Vibrational Properties of the Cs2SnX6 (X = Cl, Br, I) Defect Perovskites and Hole-Transport Efficiency in Dye-Sensitized Solar Cells. *J. Phys. Chem. C.* 120, 11777–11785. doi:10.1021/acs.jpcc.6b02175

Kojima, A., Teshima, K., Shirai, Y., and Miyasaka, T. (2009). Organometal Halide Perovskites as Visible-Light Sensitizers for Photovoltaic Cells. *J. Am. Chem. Soc.* 131, 6050–6051. doi:10.1021/ja809598r

Kumar, S., Jagielski, J., Marcato, T., Solari, S. F., and Shih, C.-J. (2019). Understanding the Ligand Effects on Photophysical, Optical, and Electroluminescent Characteristics of Hybrid Lead Halide Perovskite Nanocrystal Solids. *J. Phys. Chem. Lett.* 10, 7560–7567. doi:10.1021/acs.jpclett.9b02950

Li, J., Duan, J., Yang, X., Duan, Y., Yang, P., and Tang, Q. (2021). Review on Recent Progress of lead-free Halide Perovskites in Optoelectronic Applications. *Nano Energy*. 80, 105526. doi:10.1016/j.nanoen.2020.105526

Lin, T.-W., Su, C., and Lin, C. C. (2019). Phase Transition and Energy Transfer of lead-free Cs2SnCl6 Perovskite Nanocrystals by Controlling the Precursors and Doping Manganese Ions. *J. Inf. Display*. 20, 209–216. doi:10.1080/15980316.2019.1655493

Luo, B., Naghadeh, S. B., Allen, A. L., Li, X., and Zhang, J. Z. (2017a). Peptide-Passivated Lead Halide Perovskite Nanocrystals Based on Synergistic Effect between Amino and Carboxylic Functional Groups. *Adv. Funct. Mater.* 27, 1604018. doi:10.1002/adfm.201604018

Luo, B., Naghadeh, S. B., and Zhang, J. Z. (2017b). Lead Halide Perovskite Nanocrystals: Stability, Surface Passivation, and Structural Control. *ChemNanoMat* 3, 456–465. doi:10.1002/cnma.201700056

Maughan, A. E., Ganose, A. M., Bordelon, M. M., Miller, E. M., Scanlon, D. O., and Neilson, J. R. (2016). Defect Tolerance to Intolerance in the Vacancy-Ordered Double Perovskite Semiconductors Cs2SnI6 and Cs2TeI6. *J. Am. Chem. Soc.* 138, 8453–8464. doi:10.1021/jacs.6b03207

Mittal, M., Jana, A., Sarkar, S., Mahadevan, P., and Sapra, S. (2016). Size of the Organic Cation Tunes the Band Gap of Colloidal Organolead Bromide Perovskite Nanocrystals. *J. Phys. Chem. Lett.* 7, 3270–3277. doi:10.1021/acs.jpclett.6b01406

Nedelcu, G., Protesescu, L., Yakunin, S., Bodnarchuk, M. I., Grotevent, M. J., and Kovalenko, M. V. (2015). Fast Anion-Exchange in Highly Luminescent Nanocrystals of Cesium Lead Halide Perovskites (CsPbX3, X = Cl, Br, I). *Nano Lett.* 15, 5635–5640. doi:10.1021/acs.nanolett.5b02404

Okuda, T., Inui, K., Nakata, A., Katada, M., Terao, H., and Yamada, K. (1993). Static and Dynamic Structures of Monoalkylammonium Hexachlorostannate(IV) Complexes [CnH2n+1NH3]2 SnCl6 (N = 2 to 6) Studied by Means of NQR and NMR. *J. Mol. Struct.* 296, 103–110. doi:10.1016/0022-2860(93)80123-d

Ono, L. K., and Qi, Y. (2018). Research Progress on Organic-Inorganic Halide Perovskite Materials and Solar Cells. *J. Phys. D: Appl. Phys.* 51, 093001. doi:10.1088/1361-6463/aaa727

Pradeesh, K., Baumberg, J. J., and Prakash, G. V. (2009). Exciton Switching and Peierls Transitions in Hybrid Inorganic-Organic Self-Assembled Quantum wells. *Appl. Phys. Lett.* 95, 173305. doi:10.1063/1.3257725

Ravi, V. K., Santra, P. K., Joshi, N., Chugh, J., Singh, S. K., Rensmo, H., et al. (2017). Origin of the Substitution Mechanism for the Binding of Organic Ligands on the Surface of CsPbBr3 Perovskite Nanocubes. *J. Phys. Chem. Lett.* 8, 4988–4994. doi:10.1021/acs.jpclett.7b02192

Roy, P., Kumar Sinha, N., Tiwari, S., and Khare, A. (2020). A Review on Perovskite Solar Cells: Evolution of Architecture, Fabrication Techniques, Commercialization Issues and Status. *Solar Energy*. 198, 665–688. doi:10.1016/j.solener.2020.01.080

Saparov, B., Sun, J.-P., Meng, W., Xiao, Z., Duan, H.-S., Gunawan, O., et al. (2016). Thin-Film Deposition and Characterization of a Sn-Deficient Perovskite Derivative Cs2SnI6. *Chem. Mater.* 28, 2315–2322. doi:10.1021/acs.chemmater.6b00433

Shamsi, J., Urban, A. S., Imran, M., De Trizio, L., and Manna, L. (2019). Metal Halide Perovskite Nanocrystals: Synthesis, Post-Synthesis Modifications, and Their Optical Properties. *Chem. Rev.* 119, 3296–3348. doi:10.1021/acs.chemrev.8b00644

Stranks, S. D., and Snaith, H. J. (2015). Metal-halide Perovskites for Photovoltaic and Light-Emitting Devices. *Nat. Nanotech* 10, 391–402. doi:10.1038/nnano.2015.90

Sun, J., Yang, J., Lee, J. I., Cho, J. H., and Kang, M. S. (2018). Lead-free Perovskite Nanocrystals for Light-Emitting Devices. *J. Phys. Chem. Lett.* 9, 1573–1583. doi:10.1021/acs.jpclett.8b00301

Swarnkar, A., Chulliyil, R., Ravi, V. K., Irfanullah, M., Chowdhury, A., and Nag, A. (2015). Colloidal CsPbBr3Perovskite Nanocrystals: Luminescence beyond Traditional Quantum Dots. *Angew. Chem.* 127, 15644–15648. doi:10.1002/ange.201508276

Swarnkar, A., Ravi, V. K., and Nag, A. (2017). Beyond Colloidal Cesium Lead Halide Perovskite Nanocrystals: Analogous Metal Halides and Doping. *ACS Energ. Lett.* 2, 1089–1098. doi:10.1021/acsenergylett.7b00191

Tyagi, P., Arveson, S. M., and Tisdale, W. A. (2015). Colloidal Organohalide Perovskite Nanoplatelets Exhibiting Quantum Confinement. *J. Phys. Chem. Lett.* 6, 1911–1916. doi:10.1021/acs.jpclett.5b00664

Veronese, A., Patrini, M., Bajoni, D., Ciarrocchi, C., Quadrelli, P., and Malavasi, L. (2020). Highly Tunable Emission by Halide Engineering in Lead-Free Perovskite-Derivative Nanocrystals: The Cs2SnX6 (X = Cl, Br, Br/I, I) System. *Front. Chem.* 8, 35. doi:10.3389/fchem.2020.00035

Wang, A., Yan, X., Zhang, M., Sun, S., Yang, M., Shen, W., et al. (2016). Controlled Synthesis of Lead-Free and Stable Perovskite Derivative Cs2SnI6 Nanocrystals via a Facile Hot-Injection Process. *Chem. Mater.* 28, 8132–8140. doi:10.1021/acs.chemmater.6b01329

Wang, Q., Liu, X.-D., Qiu, Y.-H., Chen, K., Zhou, L., and Wang, Q.-Q. (2018). Quantum Confinement Effect and Exciton Binding Energy of Layered Perovskite Nanoplatelets. *AIP Adv.* 8, 025108. doi:10.1063/1.5020836

Weidman, M. C., Goodman, A. J., and Tisdale, W. A. (2017). Colloidal Halide Perovskite Nanoplatelets: An Exciting New Class of Semiconductor Nanomaterials. *Chem. Mater.* 29, 5019–5030. doi:10.1021/acs.chemmater.7b01384

Wu, X., Song, W., Li, Q., Zhao, X., He, D., and Quan, Z. (2018). Synthesis of Lead-free CsGeI 3 Perovskite Colloidal Nanocrystals and Electron Beam-induced Transformations. *Chem. Asian J.* 13, 1654–1659. doi:10.1002/asia.201800573

Xiao, K., Cui, C., Wang, P., Lin, P., Qiang, Y., Xu, L., et al. (2018). Amine Treatment Induced Perovskite Nanowire Network in Perovskite Solar Cells: Efficient Surface Passivation and Carrier Transport. *Nanotechnology* 29, 065401. doi:10.1088/1361-6528/aaa054

Xiao, Z., Zhou, Y., Hosono, H., and Kamiya, T. (2015). Intrinsic Defects in a Photovoltaic Perovskite Variant Cs2SnI6. *Phys. Chem. Chem. Phys.* 17, 18900–18903. doi:10.1039/c5cp03102h

Xie, Q., Wu, D., Wang, X., Li, Y., Fang, F., Wang, Z., et al. (2019). Branched Capping Ligands Improve the Stability of Cesium lead Halide (CsPbBr3) Perovskite Quantum Dots. *J. Mater. Chem. C.* 7, 11251–11257. doi:10.1039/c9tc03377g

Xu, Y., Li, S., Zhang, Z., Hu, Y., Yuan, L., Chen, W., et al. (2019). Ligand-mediated Synthesis of Colloidal Cs2SnI6 Three-Dimensional Nanocrystals and Two-Dimensional Nanoplatelets. *Nanotechnology* 30, 295601. doi:10.1088/1361-6528/ab13f6

Xu, Z., Mitzi, D. B., and Medeiros, D. R. (2003). [(CH3)3NCH2CH2NH3]SnI4: A Layered Perovskite with Quaternary/Primary Ammonium Dications and Short Interlayer Iodine–Iodine Contacts. *Inorg. Chem.* 42, 1400–1402. doi:10.1021/ic0261981

Yang, D., Li, X., and Zeng, H. (2018). Surface Chemistry of All Inorganic Halide Perovskite Nanocrystals: Passivation Mechanism and Stability. *Adv. Mater. Inter.* 5, 1701662. doi:10.1002/admi.201701662

Yuan, G., Huang, S., Qin, S., Wu, X., Ding, H., and Lu, A. (2019). Structural, Optical, and Thermal Properties of Cs2 SnI6 - X Br X Mixed Perovskite Solid Solutions. *Eur. J. Inorg. Chem.* 2019, 2524–2529. doi:10.1002/ejic.201900120

Zhang, F., Zhong, H., Chen, C., Wu, X.-g., Hu, X., Huang, H., et al. (2015). Brightly Luminescent and Color-Tunable Colloidal CH3NH3PbX3 (X = Br, I, Cl) Quantum Dots: Potential Alternatives for

Display Technology. *ACS Nano*. 9, 4533–4542. doi:10.1021/acsnano.5b01154

Zhang, X., Shen, J.-X., Wang, W., and Van de Walle, C. G. (2018). First-Principles Analysis of Radiative Recombination in Lead-Halide Perovskites. *ACS Energ. Lett.* 3, 2329–2334. doi:10.1021/acsenergylett.8b01297

Zhou, L., Liao, J.-F., Huang, Z.-G., Wang, X.-D., Xu, Y.-F., Chen, H.-Y., et al. (2018). All-Inorganic Lead-Free Cs2PdX6 (X = Br, I) Perovskite Nanocrystals with Single Unit Cell Thickness and High Stability. *ACS Energ. Lett.* 3, 2613–2619. doi:10.1021/acsenergylett.8b01770

Conflict of Interest: The authors declare that the research was conducted in the absence of any commercial or financial relationships that could be construed as a potential conflict of interest.